Process Safety and Environmental Protection 184 (2024) 248–259

Contents lists available at ScienceDirect

Process Safety and Environmental Protection

journal homepage: www.journals.elsevier.com/process-safety-and-environmental-protection

Numerical and experimental investigations of hydrogen-air-steam deflagration in two connected compartments with initial turbulent flow

Fangnian Wang [a], Jianjun Xiao [a,*], Sanjeev Gupta [b], Martin Freitag [b], Mike Kuznetsov [a], Shengchao Rui [a], Shangyong Zhou [a], Thomas Jordan [a]

[a] Institute of Thermal Energy Technology and Safety (ITES), Germany Karlsruhe Institute of Technology (KIT), Germany
[b] Becker Technologies GmbH, Germany

ARTICLE INFO

Keywords:
Hydrogen deflagration
Turbulent flow
Flame speed
Deflagration consequence

ABSTRACT

Turbulence in the hydrogen combustion field influences flame propagation and its consequences, which is of great importance for the safety of hydrogen/nuclear energy systems. The large-scale deflagration experiment of the premixed H_2-air-steam cloud with initial high turbulence in the large closed two-compartment system is conducted. The Computational Fluid Dynamics (CFD) tool GASFLOW-MPI developed to assess hydrogen safety during accidents, is utilized here to simulate this experiment. The objectives encompass exploring the numerical and experimental aspects of H_2 flame propagation and deflagration consequences with turbulence effect, and validating the CFD code through this experiment. The agreements between the prediction and the experimental data indicate that simulation modeling with the Large Eddy Simulation (LES) turbulence model and turbulent flame speed closure is recommended for investigating the H_2 deflagration. The experimental and predicted results indicate the following highlights. 1. The hydrogen flame can propagate in the opposite direction of the gas flow when there is an intense turbulent fluctuation upstream. 2. Turbulence accelerates the combustion velocity, causing the pressure to rise to its maximum in less than 2 s 3. So, the pre-calculation of flow turbulence before ignition and during hydrogen deflagration is essential for predicting flame propagation. 4. The peak combustion pressure increases significantly with the hydrogen concentration in a premixed lean H_2 cloud. 5. Convection and radiation contribute comparably to heat loss, leading to a decrease in system temperature and pressure. The long-term hydrogen combustion load is primarily governed by heat transfer and heat dissipation within the structures.

1. Introduction

A potential solution for reducing greenhouse gas emissions is to use vehicles powered by hydrogen produced from renewable energy (Rose, 2020). The widespread adoption of hydrogen vehicles would require numerous underground parking lots and garages. It is worth investigating the hazards associated with hydrogen fire and explosion in these closed or semi-closed systems. The hydrogen explosion accident that occurred in South Korea in 2019 highlights the importance of hydrogen safety when dealing with flammable gas mixtures in enclosed vessels, such as hydrogen storage facilities (Kim and Kim, 2019). The Fukushima nuclear accident in Japan in 2011 involved the release of combustible hydrogen resulting from nuclear core degradation, which leaked into the air-filled reactor building and led to a severe hydrogen explosion. These incidents underscore the need to comprehend the hazards posed by accidental hydrogen deflagration, especially in closed systems, and to develop appropriate models and codes for predicting premixed hydrogen deflagration.

The literature experimentally covers hydrogen deflagration, examining factors such as ignition, flame propagation, and consequence in confined vessels, addressing safety concerns (Crowl and Jo, 2007). Hydrogen detonation in H_2-air mixtures has been also explored, emphasizing the rapid and intense nature of the process (Nie et al., 2023). Research often delves into the conditions leading to detonation, shock wave, and the resulting load on containment structures (Berman, 1986; Bleyer et al., 2012). There has been significant interest in investigating the impact of flow turbulence on premixed hydrogen deflagration. Starting with the work of Damköhler (1940), the turbulent flame speed, analogous to the laminar flame speed, has been assumed to be a fundamental characteristic of premixed turbulent combustion and has

* Correspondence to: Institute of Thermal Energy Technology and Safety (ITES), Karlsruhe Institute of Technology (KIT), Hermann-von-Helmholtz-Platz 1, 76344 Eggenstein-Leopoldshafen, Germany.
E-mail address: jianjun.xiao@kit.edu (J. Xiao).

https://doi.org/10.1016/j.psep.2024.01.101
Received 30 November 2023; Received in revised form 10 January 2024; Accepted 29 January 2024
Available online 2 February 2024

been the primary focus of experimental and numerical studies (Lipatnikov and Chomiak, 2002). While existing literature provides valuable insights, a notable research gap exists. Few studies have undertaken large-scale confined, multi-compartment experiments. These experiments, encompassing various containment configurations and conditions, are essential for a comprehensive understanding of hydrogen deflagration in real-world applications.

In the framework of the early OECD/NEA THAI program (OECD/-NEA, 2010), the hydrogen deflagration behavior in the single vessel facility was investigated by varying hydrogen and steam concentrations. The current test series (THAI-HD) in this paper investigates the influence of gas stratification and initial convection flows on hydrogen combustion in a closed two-vessel/compartment system (Freitag et al., 2016 and 2018). These experiments prioritize addressing this gap to enhance our understanding of hydrogen deflagration in diverse containment settings. The provided insights and experimental database are used to develop and validate the codes for modeling hydrogen deflagration in the analytical activities of the OECD/NEA THAI-3 program.

Regarding practical requirements, the development of a predictive, reliable, and robust model for turbulent combustion in three-dimensional (3D) simulations has recently garnered significant attention. Two groups of promising models have been suggested: 1) solving the balance equation for flamelet surface density (Borghi, 1990; Boudier et al., 1992), and 2) utilizing turbulent flame speed correlations to close a balance equation for the combustion progress variable (Schmid et al., 1998; Zimont, 1979). The second method is a common practice for characterizing the combustion progress in 3D computations of premixed turbulent combustion.

Turbulent flame closures are widely used to predict the burning speed of premixed burnable mixtures. These closures, such as the Zimont correlation, were developed based on the theory of premixed combustion (Zimont, and, 1979, 2000; Lipatnikov and Chomiak, 2002). The correlation depends on the physicochemical properties of the combustible mixtures and flow turbulence. Turbulent flame closures have been implemented in many Computational Fluid Dynamics (CFD) tools, such as CFX, FLUENT, OpenFOAM, GASFLOW-MPI, and validated against hydrogen deflagration experiments (Gerke and Boulouchos, 2012; Xiao et al., 2015; Halouane and Dehbi, 2017; Povilaitis and Jaseliūnaitė, 2021). These CFD calculations, which couple the Zimont correlation with minor adjustments of the scaling factor, agree well with experimental data, revealing their reliability in modeling the turbulent burning velocity. Turbulent kinetic energy is usually modeled using the Reynolds-averaged (RANS) turbulence model in the turbulent kinetic energy equation. However, turbulent energy can be resolved directly using the Large Eddy Simulation (LES) method over a wide range of scales, with only the turbulence fluctuation at the sub-grid scale being modeled by the SGS (sub-grid scale) model. The time-averaged RANS model for turbulence quantities is valid only if the time-scale of the turbulent fluctuations is much smaller than the combustion process time-scale. Therefore, compared to the RANS turbulence model, the LES turbulent model is less sensitive to modeling errors (Salmanzadeh et al., 2010).

GASFLOW-MPI is the advanced parallel version of the GASFLOW sequential code with many newly developed models and features, validated by numerous international benchmarks on shock waves, premixed/non-premixed turbulent combustion, and detonations in tubes, demonstrating its reliability in predicting all speed flow-fields associated with hydrogen safety, including heat and mass transfer (Xiao et al., 2016, 2017). The significant advantage of the GASFLOW-MPI code lies in its all-speed capability to simulate laminar and turbulent distribution processes, slow deflagration, transition to fast hydrogen combustion modes, including detonation, all within a single scientific software framework. This eliminates the need to transform data between different solvers or codes. Nevertheless, there is still room for further validation of GASFLOW-MPI when utilized in large-scale experiments, especially involving turbulence initialization before ignition.

Therefore, the objectives of this paper include the following aspects:

- Investigate experimentally and numerically the H_2 flame propagation and the deflagration consequences in large-scale multi-compartment with initial turbulence.
- Validate the CFD code through those H_2 deflagration experiments.

As mentioned earlier, this paper aims to conduct numerical and experimental investigations of the deflagration of premixed H_2-air-steam mixtures in the large-scale THAI+ facility. It also discusses the turbulence effect on hydrogen flame propagation and its impact on the resulting pressure and temperature load.

2. Numerical model

GASFLOW-MPI is a parallel finite-volume CFD code that adopts the Implicit Continuous Eulerian - Arbitrary Lagrangian Eulerian (ICE'd-ALE) solution algorithm (Xiao et al., 2016). GASFLOW-MPI is applicable to all speed flows, from incompressible to supersonic flow regimes, allowing the simulation of major hydrogen safety-related phenomena, such as release, turbulent dispersion, deflagration, and detonation. The progress variable combustion model, the LES turbulence model for computing premixed turbulent combustion are described, and the heat transfer model, are briefly presented, respectively.

2.1. Progress variable combustion model

In order to model the flame front propagation and track the global extent-of-reaction of the local mixture, the transport equation of the density-weighted mean reaction progress variable, ξ, is solved (Xiao et al., 2016),

$$\frac{\partial}{\partial t}(\rho\xi) + \nabla\cdot(\rho\xi\boldsymbol{u}) = \nabla\cdot\left[\left(\rho\alpha_u + \frac{\mu_t}{Sc_t}\right)\nabla\xi\right] + \rho S_\xi, \tag{1}$$

where ρ is the density, $\boldsymbol{u}$ is the velocity, t is the time, α_u is the thermal diffusivity of the unburned mixture, μ_t is the turbulent dynamic viscosity, Sc_t is the turbulent Schmidt number. For hydrogen-fueled mixtures, the mean combustion progress variable, ξ, is usually written as,

$$\xi(\boldsymbol{x}, t) = \frac{Y_{H_2,unburned}(\boldsymbol{x}, t) - Y_{H_2}(\boldsymbol{x}, t)}{Y_{H_2,unburned}(\boldsymbol{x}, t) - Y_{H_2,burned}(\boldsymbol{x}, t)}, \tag{2}$$

where $\boldsymbol{x}$ is the position vector, Y represents the hydrogen mass fraction in unburned and burned zones. Obviously, the progress variable, $\xi = 1$ in the burnt mixture and $\xi = 0$ in the unburnt mixture.

The key to the approach is how to solve the source term, ρS_ξ. In fact, GASFLOW-MPI provides various concepts for modeling this source term, each with its own specific assumptions. For example, the Arrhenius rate model neglects the turbulence effect, and the eddy dissipation model assumes combustion occurs at a small scale where the fuel and oxidizer mix on the molecular scale with sufficiently high temperature (Magnussen and Hjertager, 1977). The method based on the progress variable gradient would be better suited for the current problem – H_2 deflagration with initial turbulence in large-scale experiments. The source term of the mean reaction progress variable equation can be modeled as,

$$\rho S_\xi = \rho_u S_T|\nabla\xi| = \rho_u S_T\sqrt{\frac{\partial\xi}{\partial x} + \frac{\partial\xi}{\partial y} + \frac{\partial\xi}{\partial z}}, \tag{3}$$

where ρ_u is the density of unburnt mixture, and S_T is the turbulent flame speed. In order to implement this approach, a suitable flame speed closure of S_T is required. GASFLOW-MPI provides several correlations for turbulent flame speed, according to our previous study (Wang et al., 2022a; Wang et al., 2023), the Zimont model (Zimont, 1979) is recommended to calculate the wrinkled flame fronts at high turbulence,

$$S_T = 0.52(u_t^{'})Da^{0.25}, \quad (4)$$

where the integral turbulent velocity fluctuation $u_t^{'} = \sqrt{\frac{2}{3}\kappa}$, where the κ is the turbulent kinetic energy. Damköhler number, $Da = \frac{\tau_t}{\tau_c}$, is defined as the ratio of the turbulent integral timescale τ_t to the chemical timescale τ_c. The turbulent integral timescale, $\tau_t = \frac{l_t}{u_t^{'}}$, and the chemical timescale is defined as $\tau_c = \frac{\alpha}{S_L^2}$, where α is the gas thermal diffusivity.

The thermal diffusivity of the unburned gas is modified in terms of pressure and temperature as well,

$$\alpha_u = \alpha_{u,0} \left(\frac{P_u}{P_{u,0}}\right)^{\phi}\left(\frac{T_u}{T_{u,0}}\right)^{\lambda}, \quad (5)$$

where $P_{u,0}$, $T_{u,0}$ and $\alpha_{u,0}$ are the initial pressure, temperature and thermal diffusivity of the unburned mixture, respectively.

The laminar flame speed S_L is corrected by local pressure and temperature. The compression of unburned gas ahead of the flame may increase the pressure and temperature. Taking the effects of compression into account, the thermo-dynamic correlation of the laminar flame speed S_L can be expressed (Metghalchi and Keck, 1982) with the exponents of hydrogen,

$$S_L = S_{L,ref} \left(\frac{P_u}{P_{ref}}\right)^{a}\left(\frac{T_u}{T_{ref}}\right)^{b}, \quad (6)$$

where P_u and T_u are the pressure and temperature of the unburned mixtures, respectively. The reference laminar flame speed is,

$$S_{L,ref} = \left(1.44\phi^2 + 1.07\phi - 0.29\right)(1-\varphi)^4, \quad (7)$$

where a and b are the function of the equivalence ratio ϕ; φ is the diluents' (e.g. steam, He, CO_2 etc.) volume fraction, and $S_{L,ref}$ is the laminar flame speed at the reference pressure $P_{ref} = 101325$ Pa and temperature $T_{ref} = 298$ K.

2.2. LES turbulence model

The large eddy simulation of reacting and non-reacting flows often require the estimation of the sub-grid scale (SGS) turbulence kinetic energy, κ, or the sub-grid velocity scale (integral turbulent velocity fluctuation) $u_\Delta^{'} = u_t^{'} = \sqrt{2\kappa/3}$. This quantity can be computed using a transport equation for κ, for example, in the well-known $k-\varepsilon$ model (Launder and Rodi, 1983), which, however, leads to additional unclosed terms and computational cost so that it is not the preferred choice in a large eddy simulation (Langella et al., 2018). The turbulence fluctuation in LES can be modeled by SGS model. The residual stresses are modeled as sub-grid turbulent stresses with an eddy viscosity assumption. The SGS Reynolds stresses term $\widetilde{\sigma}_{ij}$ in Navier-Stokes equations with the Boussinesq hypothesis can be expressed as,

$$\widetilde{\sigma}_{ij} = -2\mu_t S_{ij} + \frac{2}{3}\kappa\delta_{ij}, \quad (8)$$

where the rate-of-strain tensor $S_{ij} = \left(\partial u_i/\partial x_j + \partial u_j/\partial x_i\right)/2$ and δ_{ij} is Kronecker delta.

The Smagorinsky model is employed in GASFLOW-MPI to calculate the SGS turbulent viscosity due to its simplicity and practicality (Zhang et al., 2017). The turbulent viscosity in the Smagorinsky model, is proposed by assuming that the turbulent energy transfers from the large resolved scales to the small sub-grid scales and the turbulent energy dissipation by the small sub-grid scales are in equilibrium (Smagorinsky, 1963; Piomelli, 1999). The μ_t SGS turbulent viscosity is,

$$\mu_t = \rho {l_t}^2|S|, \quad (9)$$

where the inner product of strain rate tensor $|S| = \sqrt{2\overline{S}_{ij}\overline{S}_{ij}}$ and the turbulent length scale l_t is,

$$l_t = C_S\Delta \ based\ on\ \Delta = \left(\Delta_x\Delta_y\Delta_z\right)^{1/3}, \quad (10)$$

C_S is a constant in Smagorinsky model that depends on the flow pattern (Hassan, 2008). $C_S = 0.1$ is recommended for the best estimate in simulations. Δ is the LES filter width, which is computed from the size of the computational cells. The turbulent viscosity is a function of the mesh size. The sub-grid scale velocity $u_\Delta^{'}$ that is used for computing the turbulent flame speed is,

$$u_\Delta^{'} = l_t\sqrt{2\overline{S}_{ij}\overline{S}_{ij}}, \quad (11)$$

2.3. Heat transfer model

2.3.1. Convective heat transfer and phase change

The convective heat transfer between the high-temperature gas produced by the hydrogen combustion and the containment wall is,

$$S_{\rm conv} = h_w A_{\rm w}\left(T_{\rm w} - T_{\rm g}\right), \quad (12)$$

where $S_{\rm conv}$ is the convective heat transfer, h_w is the heat transfer coefficient between the wall and the high-temperature gas, $A_{\rm w}$ is the exposed area of the inner wall of the calculation unit, $T_{\rm w}$ is the wall temperature, and $T_{\rm g}$ is the high-temperature gas temperature.

The rate of phase change on a structural surface can be described as follows,

$$\dot{m}_s = \Theta_m h_d A_{\rm w}\left(\rho_{\rm h_2o} - \rho_{s,\rm sat}\right), \quad (13)$$

where h_d^* is the corrected mass-transfer coefficient, $\rho_{\rm h_2o}$ is the water vapor density in the gas mixture, and $\rho_{s,\rm sat}$ is the saturation water vapor density at the structural surface. The saturation density is computed from the saturation pressure and the structural surface temperature $\rho_{s,\rm sat} = \frac{p_{s,\rm sat}(T_s)}{R_{\rm h_2o}\cdot T_s}$, where the saturation pressure is evaluated as a function of temperature from the integrated Clausius-Clapeyron equation$p_{\rm sat}(T) = 10^6\cdot e^{\frac{-c_1+c_2\cdot T}{c_3\cdot T}}$. The correction factor $\Theta_m = \frac{\log(R+1)}{R}$. The relaxing ratio R is expressed as $R = \frac{n_{s,\rm h_2o} - n_{\rm h_2o}}{1-n_{s,\rm h_2o}}$. $n_{s,\rm h_2o}$ is the steam mole fraction at the wall, and $n_{\rm h_2o}$ is the steam mole fraction in the gas mixture.

To model the convective and phase change coefficients, Reynold analogy is adopted for calculating heat transfer, while Chilton-Colburn empirical analog is used to model mass transfer. The convection heat transfer coefficient and the condensation/vaporization coefficient are,

$$h_w = \frac{\rho c_p u^*}{u^+}{\rm Pr}^{-\frac{2}{3}}, \quad (14)$$

$$h_d = \frac{h_w}{\rho c_p}\left(\frac{Sc}{\rm Pr}\right)^{-\frac{2}{3}}, \quad (15)$$

Both coefficients should be corrected by the steam mass/mole fractions. u^* is wall shear velocity and u^+ is dimensionless velocity, $u^+ = u_c/u^*$, u_c is cell-center fluid velocity.

2.3.2. Thermal radiation

Thermal radiation emitted by combustion products can significantly impact the combustion and heat transfer processes. A computationally efficient thermal radiation transport model has been developed in GASFLOW-MPI code. In situations where photon scattering is absent, and the gas is assumed to reach locally thermodynamic equilibrium, the thermal radiation transport equation for a gray gas has been presented in previous studies (Chandrasekhar, 1960; Sparrow and Cess, 1978; Siegel and Howell, 1992),

$$\frac{1}{c}\frac{\partial E(\boldsymbol{r},\Omega,t)}{\partial t}+l_i\frac{\partial E(\boldsymbol{r},\Omega,t)}{\partial x_i}=-\alpha E(\boldsymbol{r},\Omega,t)+\frac{\alpha\sigma T^4}{\pi}, \tag{16}$$

where the absorption coefficient is denoted by α, the speed of light by c, the Stefan-Boltzmann constant by σ, and the temperature of the gas by T. The specific radiant intensity, $E(\boldsymbol{r},\Omega,t)$, is a function of the position vector $\boldsymbol{r}$, directional vector Ω, and time t. l_i is the direction cosines of the vector Ω with respect to the coordinate directions x_i. This equation can be approximated by a set of differential equations by means of the "moment" or "differential" approximation method. The moment approximation equations can be expressed in terms of the radiant energy density $U^r=\frac{1}{c}\int\Omega E(\boldsymbol{r},\Omega,t)d\Omega$ and the radiant flux vector $q_i=-\frac{c\lambda}{3}\frac{\partial U^r}{\partial x_i}$,

$$\frac{\partial U^r}{\partial t}+\frac{\partial q_i}{\partial x_i}=\frac{c}{\lambda}\left(\alpha T^4-U^r\right). \tag{17}$$

The absorption coefficient α is the reciprocal of the photon "mean free path", $\lambda=\frac{1}{\alpha}$. To provide the proper coupling between the fluid and thermal radiation transport equations, the expression on the right-hand side of Eq. (17) multiplied by negative one, is used in the internal energy transport equation on the right-hand side,

$$\frac{\partial}{\partial t}(\rho I)+\nabla(\rho\boldsymbol{u}I)=-p\nabla\boldsymbol{u}-\nabla\boldsymbol{q}+Q-\frac{c}{\lambda}\left(aT^4-U^r\right), \tag{18}$$

where I is the mixture specific internal energy, and $\boldsymbol{q}$ is the Internal energy flux vector.

3. Experiment and simulation set-up

3.1. Experiment facility

The THAI facility was originally designed to investigate containment phenomena, such as thermal-hydraulic, aerosol, and iodine behavior during severe accidents in nuclear power plants. Multiple national (BMWi) and international (OECD/NEA) tests have been conducted in this facility (Gupta et al., 2021). The design pressure is 14 bar, and the temperature is 180 °C, allowing for hydrogen deflagration tests. The obtained experimental data are used to develop and validate Lumped-Parameter (LP) codes and CFD codes. In 2015, the facility was expanded with an additional cylindrical vessel called THAI+ , as shown in Fig. 1. The Parallel Attachable Drum (PAD) is connected to the former THAI Test Vessel (TTV) by both upper and lower connecting pipes with a diameter of 0.5 m. The expanded THAI+ allows for research on multi-compartment geometry effects on hydrogen deflagration phenomena (Freitag et al., 2016).

The TTV has a height of 9.2 m and a diameter of 3.2 m, with a free volume of approximately 60 m^3, while the PAD has a height of 10 m, a diameter of 1.55 m, and a free volume of 18 m^3. Several components, such as the fan, condensate trays, and inner cylinder, can be removed according to the experimental setup requirements. The condensate trays and inner cylinder are removed in the hydrogen deflagration test HD-44 of interest in this paper. The facility is thermally insulated by a 120 mm thick layer of rock wool. The main cylindrical parts of TTV and PAD, except for the connecting pipes, can be heated or cooled individually by three oil mantle systems.

3.2. Experimental procedure

Before commencing data acquisition, the THAI+ facility was heated using thermal oil mantles and all electrical heaters. The electrical heaters were set to 90 °C and activated until the corresponding wall temperatures dropped below 90 °C. Once the temperature of the respective control thermocouple reached 90 °C, the heaters were deactivated. The initial gas mixture was prepared by injecting air and steam. The blower was activated during the steam injection. Subsequently, the blower was operated at 50 Hz under a constant pressure of 1.525 bar, while velocities were measured inside the upper connecting pipe. This was followed by a gas relief operation to reduce vessel pressure.

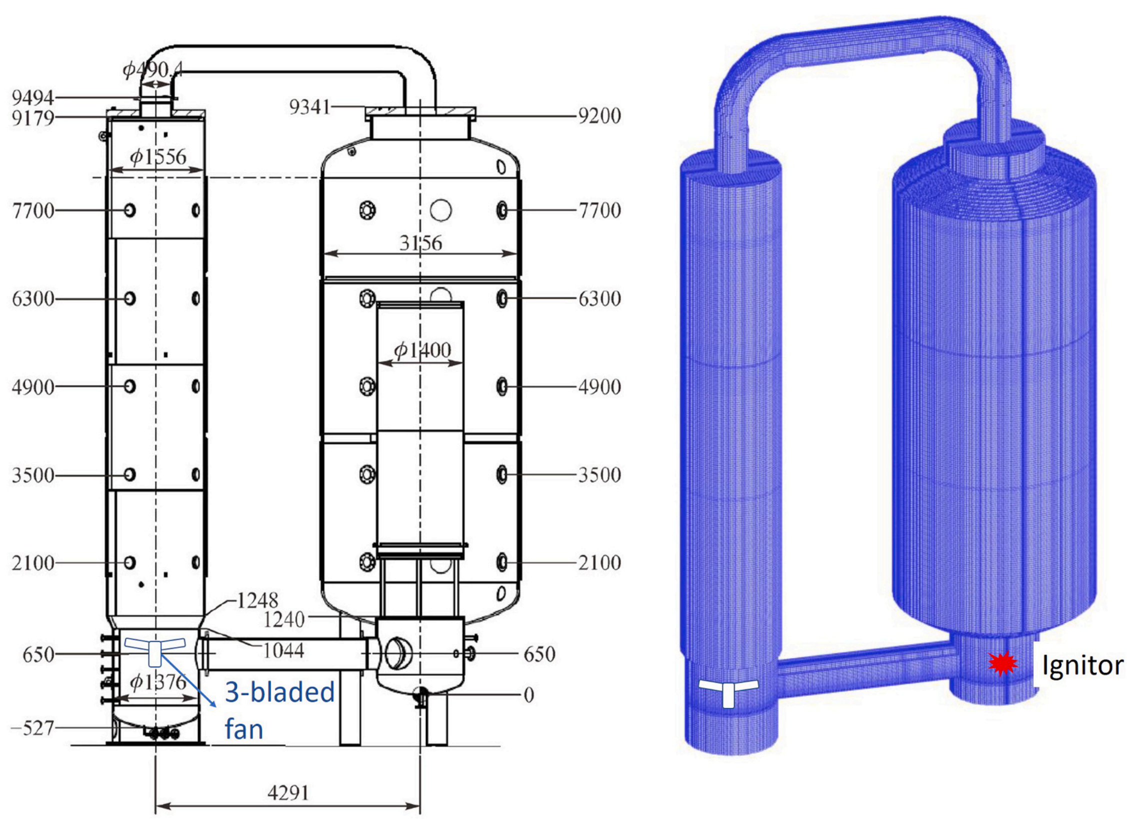

Fig. 1. THAI+ facility and the computational mesh (>12 Million cells).

Hydrogen was then injected and mixed by the blower. The main test phase commenced with the activation of the igniter.

The pressure evolution during the hydrogen deflagration is measured by fast strain gauge pressure transducers. Atmosphere and structure temperatures are measured by numerous slow and fast thermocouples. The slow thermocouples have a diameter of 1.5 mm and an actual response time of 1100 ms, while the fast thermocouples have a diameter of 0.5 mm and an actual response time of 210 ms. The igniters are installed at an elevation of 0.5 m in the sump compartment of the TTV vessel, and controlled remotely. The ignition sequence has a duration of 1 s, and the integral energy is approximately 10 J. The maximum delay time between starting the igniter and delivery of the first spike is around 40 ms. Initial conditions are provided at the start of ignition, t = 0 s. The initial conditions of pressure, gas and wall temperatures, steam and hydrogen volume concentrations are given in Table 1. In the test, the three-bladed fan operates at a speed of 715 rpm (revolutions per minute). The gas mixture is drawn from the PAD vessel and blown into the sump compartment, and subsequently through the lower connecting pipe into the TTV vessel. More experimental details can be found in the reference (Freitag et al., 2018).

3.3. Simulation set-up

The 3D grid of the THAI+ geometry is generated in Cartesian coordinates. The computational domain is resolved by a total number of 12,297,494 hexahedral grid cells, with 251,131 and 374 cells in the x, y, and z directions, respectively, as shown in Fig. 1. However, the vessel is located in a larger computational domain in order to simulate heat transfer through the vessel walls. The cell size of the THAI+ vessel is 2.5 cm. Mesh sensitivity analysis will not be performed in this article, as 12 million grids provide a fine mesh resolution for the current calculation. The areas of the fan location, ignition position, and the connection pipe are refined, as seen in the mesh figure in supplementary data. These zones are of great importance in simulating turbulence and flame propagation.

Test HD-44 was performed in H_2-air-steam mixtures with an initial turbulent flow. The gas mixture is driven by the fan, which ignites at the bottom of the TTV vessel. The ignition in the simulation is initiated as a high-temperature cell within a short time duration (10^{-5} s). The fan, with a rotational speed of 715 rpm, is modeled as a velocity boundary in the area around the fan blades. The fan model is set up to allow the gas at the bottom of the PAD to pass through the fan blades to the vessel THAI. Velocity and turbulence fields at the bottom of the PAD are obtained with the fan model and are verified by the experimental data. The fan model in our code is set up through a set of velocity boundary conditions. See the details in supplementary data.

The heat transfer in the vessel walls is modeled as one-dimensional thermal conduction, perpendicular to the structure's surface. The conductor is a combination of stainless steel, insulation, and aluminum thicknesses defined in the THAI+ configuration geometry. Heat transfer between the gas and structure surfaces is modeled by convective heat transfer, phase change, and thermal radiation. A non-slip boundary condition is applied to the walls of all the components of the facility. The LES turbulence model and the turbulent flame speed closure are adopted. The well-known second-order accuracy Van Leer scheme has been employed for the discretization of the convective terms. The time step has been restricted to a maximum permitted time step of 10^{-4} s, corresponding to a maximum Courant-Friedrichs-Lewy (CFL) number of 0.25. The simulation took 43 h using 128 processors for a total problem time of 20 s.

Fig. 2 right side depicts the experimental mean stream-wise velocity flow profile and the corresponding fluctuations recorded and averaged over one complete turn of the velocity measurement device. The average stream-wise velocity inside the upper pipe was measured to be 6.43 m/s, with a minimum velocity of 4.74 m/s and a maximum velocity of 7.36 m/s. The corresponding average velocity fluctuation was 0.244 m/s. To ensure an accurate initial velocity field, the distribution of initial velocities at the time of ignition, as well as the distribution of turbulent fluctuation, were determined through pre-calculation, as shown in Fig. 2 left side and the full scope in Fig. 3. In the upper connection tube, the predicted velocity distribution profile is quite similar to the experiment. The predicted maximum velocity is higher than the measurement. The bias of the turbulent fluctuation between the experimental and calculated data is relatively larger than the velocity distribution, but both fluctuation ranges are in around 0–0.7 m/s. Generally, the results demonstrate an agreement between the initial velocity and turbulent fluctuation inside the upper pipe and the measured values. Consequently, the predicted velocity field before ignition can be utilized to initialize the simulation of hydrogen deflagration in the HD-44 test.

Table 1
Measured initial conditions of THAI-HD-44 test.

Pressure, bar	1.46
Average temperature, °C	89
Hydrogen concentration, vol%	10.21
Steam concentration, vol%	25
TTV/PAD wall temperature, °C	90.8/89.1
Upper/Lower pipe wall temperature, °C	84.3/79.8
Fan velocity, rpm	715

4. Result and discussion

4.1. Flame propagation

- **Potential of deflagration**

H_2-air mixtures may be diluted with another gas (such as steam) until the hydrogen is no longer flammable. This composition determines whether the mixture is flammable or non-flammable, defined as the flammability limit, as well as the detonation limit. A combustible gas mixture generally has an upper limit and a lower limit of hydrogen flammability and detonation. The gaseous mixture will only burn or explode when its composition is within these limits. For H_2-air mixtures, the flammability upper and lower limits are typically quoted as 4.1 and 74 vol% hydrogen concentration, respectively (Shapiro and Moffette, 1957). However, these limits depend on the mixture's temperature and pressure. If the lower limit of flammability is raised to 19 vol% and the upper limit is lowered to 54 vol%, detonation could occur (Shapiro and Moffette, 1957). It is important to note that the potential for flame propagation or detonation decreases as the dilution gas concentration increases. The flame can even be extinguished by diluting with a high concentration of gas (e.g., 60 vol% steam in H_2-air mixtures).

The Shapiro Diagram is often used to illustrate the potential for flame propagation of a combustible gas mixture. The initial gas volume fraction in test HD-44 is plotted on the Shapiro Diagram under standard conditions (25 °C and 1 bar, Coward and Jones, 1952), as well as other higher temperature and pressure conditions (Shapiro and Moffette, 1957), as shown in Fig. 4 left subfigure. The differences in flammability and detonation limits under different conditions are not significant. The gas temperature and pressure are approximately 88 °C and 1.5 bar, respectively. The placement of H_2-air-steam mixtures on the Shapiro Diagram indicates the potential for deflagration in test HD-44. However, the Shapiro Diagram cannot reveal the impact of turbulence on hydrogen flame propagation.

- **Combustion regime**

The Borghi diagram (Borghi, 1985) illustrates a classification into five combustion regimes based on the dimensionless turbulent Reynolds number ($Re_t = \frac{u_t' l_t}{\nu}$), Karlovitz number ($Ka = \left(\frac{u_t'}{S_L}\right)^2 Re_t^{-0.5}$), and Damköhler number ($Da = \frac{l_t S_L^2}{u_t' \alpha}$), as shown in Fig. 4 right subfigure.

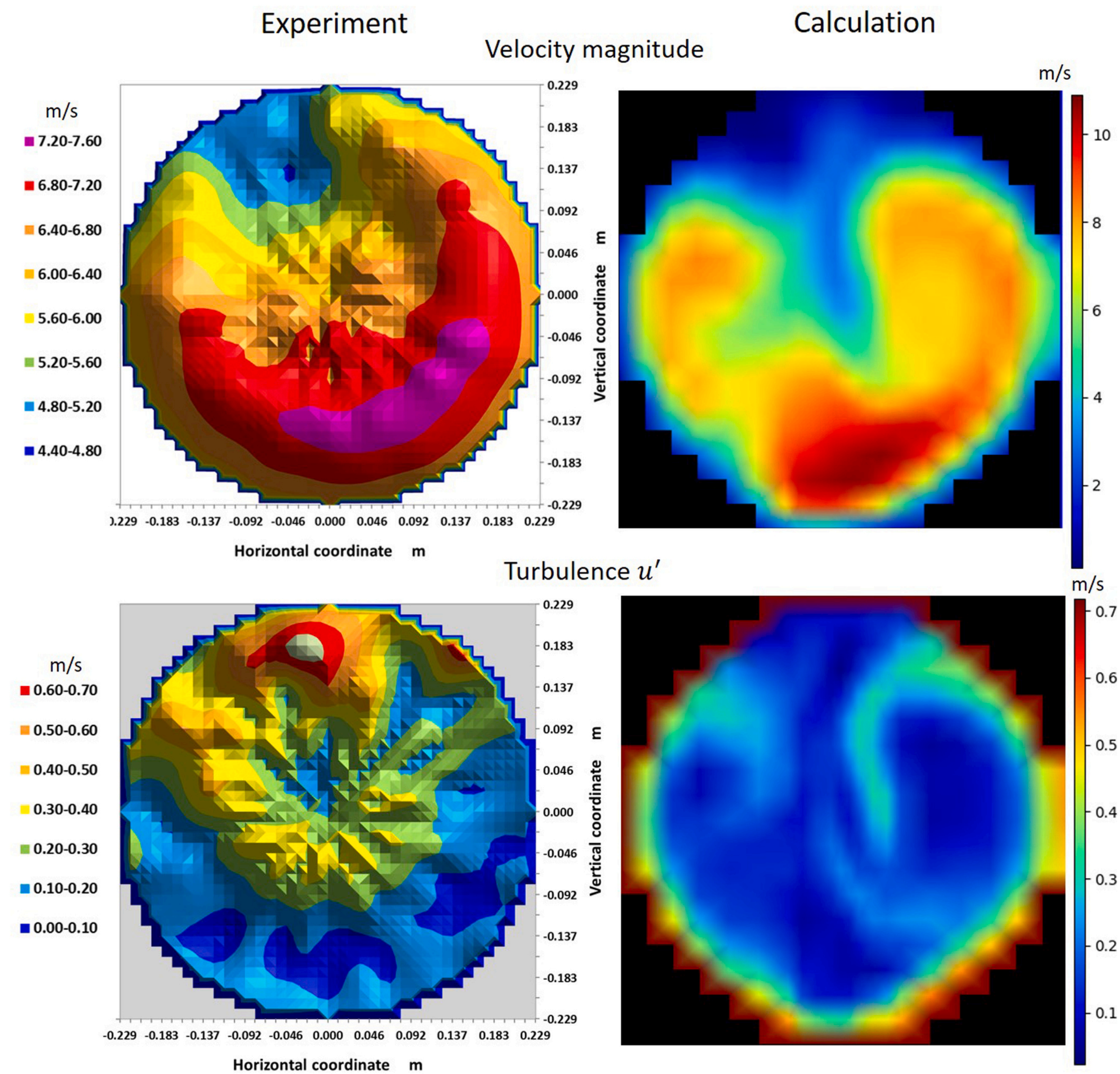

Fig. 2. Comparisons of initial velocity and turbulent fluctuation in the upper connection pipe in test HD-44.

Faix-Gantier (2001) estimated that, in the case of a moderate hydrogen release accident, the integral length scale would vary in the range of 0.02 - 2 m and the turbulent intensity from 0.03 - 15 m/s, which contains the test HD-44 initial conditions. Considering the lean H_2 mixture, the laminar premixed flame speed usually increases with the hydrogen concentration, but up to 2 m/s if the equivalence ratio is less than 1 (Sathiah et al., 2012). Thus, the corresponding combustion regimes of THAI-HD-44, follow the area gray-colored area in Fig. 4 right subfigure. The flame thickness on the x-axis is defined as $\delta = \frac{\alpha}{S_L}$.

According to the initial test conditions of HD-44, the flame propagation starts in the wrinkled flamelets regime ($\mathrm{Re}_t > 1$ and $\frac{u_L'}{S_L} < 1$). With an increase in turbulent intensity during the combustion, the wrinkled flame could convert into the corrugated flamelets regime ($\frac{u_L'}{S_L} > 1$ and $Ka < 1$), which is associated with highly convoluted, multiple connected flamelets, or further into the thickened wrinkled flames regime ($Ka < 1$ and $Da > 1$), where the chemical reactions control heat release process in a thick distributed zone comparable to the integral length scale. The increase in turbulence is also possibly due to the geometry obstacle or deformation, e.g., in the vessel dome connecting a pipe. It is easier to observe the change of combustion regime at the entrance of the pipe than in the balk of the vessel, as seen in the following flame propagation discussion.

- **Flame propagation in the system**

The gas mixture is ignited at the bottom of the TTV vessel, resulting in a flame propagating upward and simultaneously through the lower connecting pipe to the PAD vessel. Fig. 5 presents the development of the temperature field, the progress variable ξ, and the turbulence

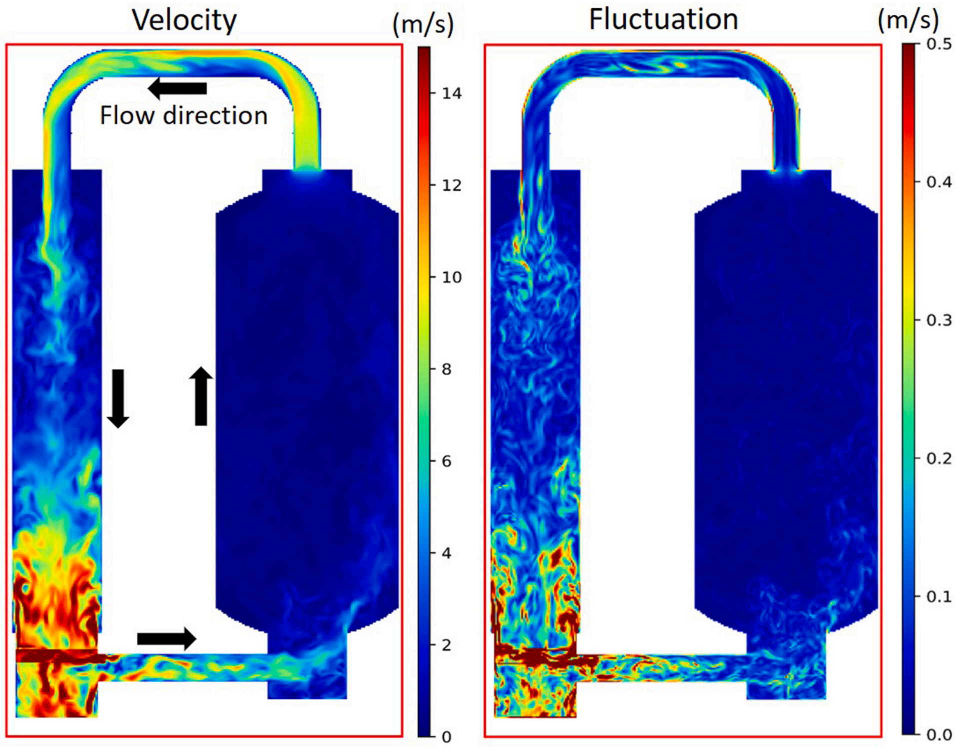

Fig. 3. Distribution of initial velocity (left) and turbulent fluctuation (right) in test HD-44.

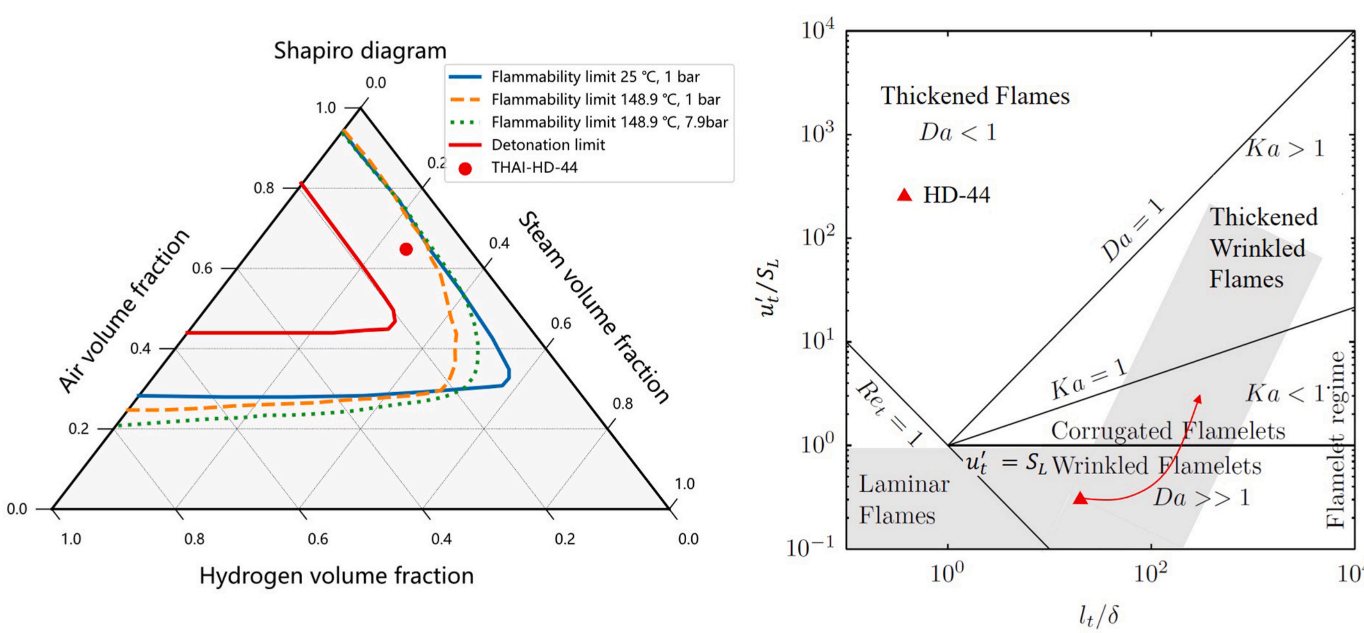

Fig. 4. Shapiro Diagram (left) and Borghi Diagram (right).

fluctuation after ignition in test HD-44. The hydrogen concentration distribution exhibits a similarity to the contours of the progress variable field. The temperature contour almost overlaps the flame front, where the progress variable boundary between the burned and unburned mixture is located. However, the temperature experiences a step change at the flame front, while there is an obvious gradient of the progress variable.

The flame passes through the lower connecting pipe and continuously propagates upward in the PAD vessel. The hydrogen flame propagates in the opposite direction of the gas flow, as there are intense turbulent fluctuations in the upstream flow, as shown in Fig. 5. The flame meets in the upper connecting pipe and ends its combustion in the top dome of the TTV vessel. The hydrogen burns almost completely in 2 s. The flame brush thickness, which characterizes the transition zone between the unburned and burned states of a premixed flame, is pronounced at the flame front, as shown by the gradient in the contours of the progress variable ξ. The flame brush thickness depends on the distribution of turbulence intensity.

A detailed comparison of isochrones representing the propagation of the flame front throughout the TTV and PAD configuration is presented

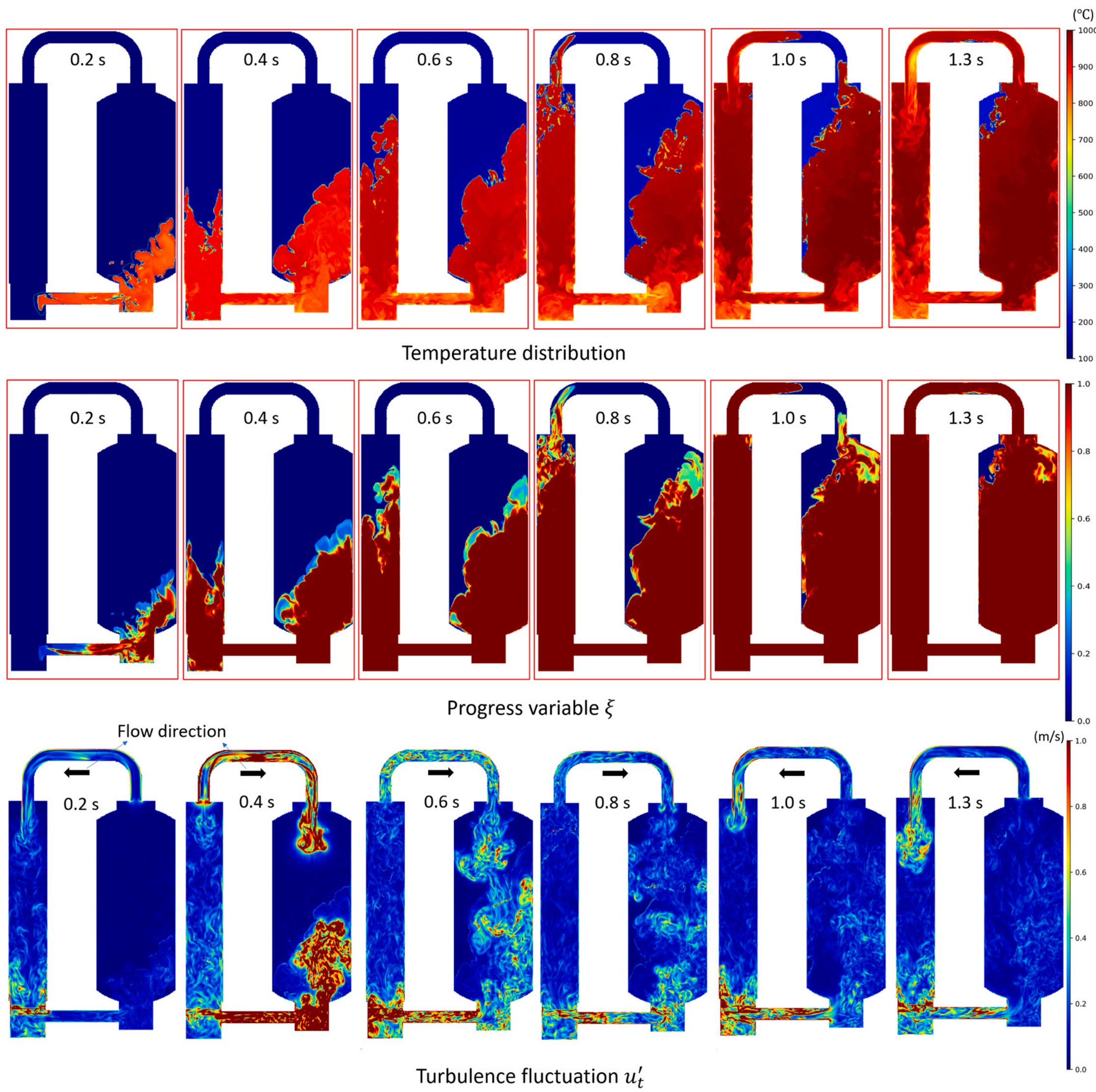

Fig. 5. Developments of the temperature (top), progress variable ξ (middle), and the turbulence fluctuation (bottom) after ignition in test HD-44.

in Fig. 6. The predicted isochrones are extracted from the interfaces of burned and unburned gas in Fig. 5, temperature contours. The initial fast rise of the temperature sensor (experimental isochrones) indicates the flame front passing the thermocouple. The flame in the TTV propagates more or less continuously in ascending order along the centerline of the TTV approximately, which is consistent with the calculation results qualitatively. A similar upwards flame travel was recorded for the PAD vessel, but here against the circulating flow field resulting in a V′ type of the front shape until approximately H = 5.6 m, where the flame seems to rest for a while (~0.3 s) in the experiment. Thereafter, the upper half of the PAD and the upper connecting pipe show a very fast burn up (Freitag and Sonnenkalb, 2019).

Furthermore, the impact of turbulence fluctuation on flame speed can be observed in the flame traveling along the vessel axis of the TTV and PAD, as shown in Fig. 7. The flame speed is around 10 m/s in the TTV vessel, while it is around 20 m/s in the PAD vessel, since the initial turbulence velocity in the PAD vessel is much larger than that in the TTV vessel (as seen in Fig. 3 right subfigure). Turbulence can increase the reaction area, heat, and mass transfer, thereby increasing the flame speed. This result is consistent with indications from various previous experimental investigations (Lipatnikov and Chomiak, 2002), namely the behavior of turbulent flame speed S_T, which increases with turbulent velocity $u_t^{'}$ under moderate turbulence.

Fig. 7 and Fig. 8 compare the simulation results of the flame propagation along the vessel centerlines and along the connecting pipes with the experimental data, indicating that the simulations reproduced the experimental data quite well. The flame propagates faster in the PAD vessel (~20 m/s) than in the TTV vessel (~10 m/s). The flame propagation in the PAD starts 0.2 - 0.3 s later than in the TTV due to the time delay caused by the flame traveling through the lower connecting pipe. However, the flame in the PAD catches up with the flame in the TTV at a middle elevation of around 5 m. The CFD prediction once again agrees that the flame in the PAD propagates faster and reaches the upper connecting pipe before the flame in the TTV. In Fig. 8, the positive slope of the lower connecting pipe curve indicates that the flame travels from the TTV to the PAD and vice versa. The flame speed around the meeting position slows down due to the suppression of momentum from both sides.

4.2. Pressure response

The hydrogen combustion can result in high-pressure and -temperature loads on the containment vessel. The combustion phase begins with the ignition of the gas mixture at t = 0 s. The vessel pressure rises to approximately 4.65 bar within 1.4 s in test HD-44, as shown in Fig. 9. The time until reaching the peak pressure is considerably fast, because

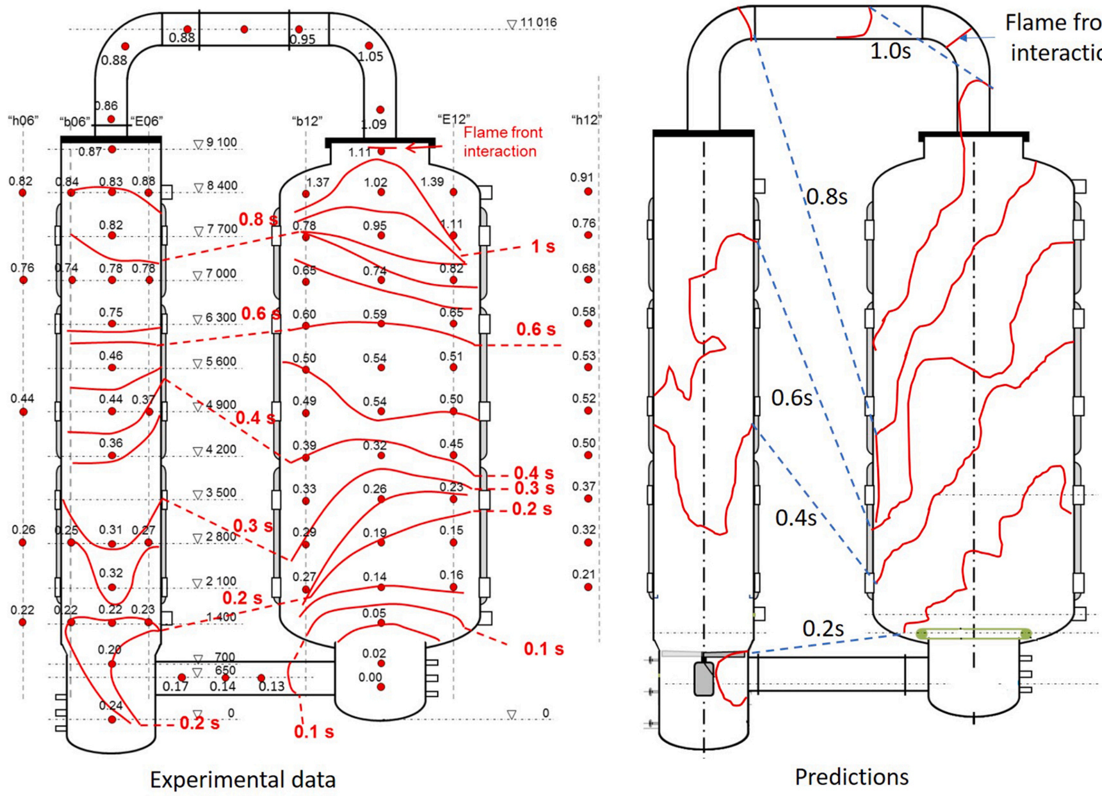

Fig. 6. Comparison of the flame front propagation as isochrones in test HD-44.

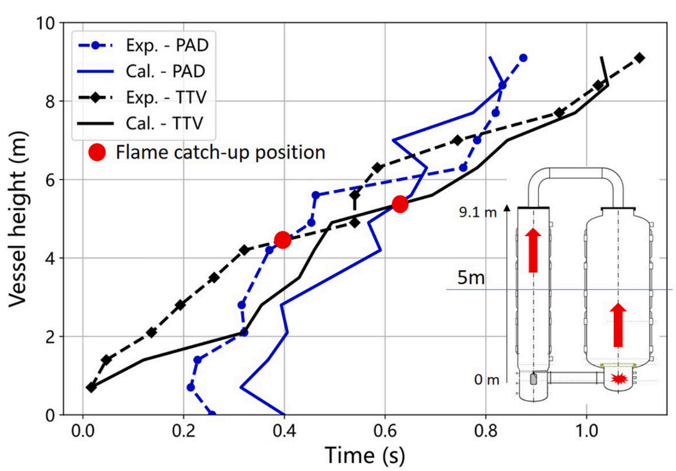

Fig. 7. Flame propagating along the vessel axis of the TTV and PAD in test HD-44 with all results shifted to a flame propagation start at t = 0 s.

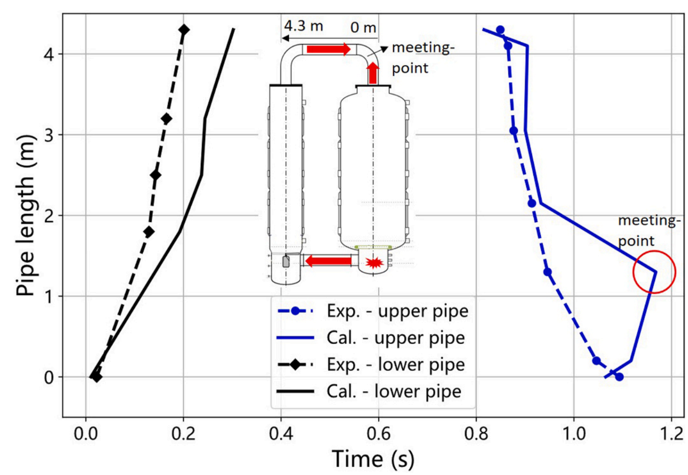

Fig. 8. Flame propagating between TTV and PAD through the upper and lower connecting pipes in test HD-44.

the speed of hydrogen combustion depends highly on the turbulence intensity. Once the flame becomes turbulent, the flame speed increases continuously with increasing turbulence intensity.

Generally, the pressure transient can be divided into two phases: pressure-rising and pressure-decreasing. During the pressure rising phase, the release of reaction heat is rapid in a short time (< 2 s), and heat loss is little, resulting in an increase in pressure, as seen in the heat loss discussion. The rate of pressure rise depends on the combustion speed. When the release of reaction heat is balanced by heat loss, the pressure reaches its peak. The subsequent pressure decrease is due to continuous vessel cooling. Comparisons show that GASFLOW-MPI is capable of reproducing the pressure transient (as well as in the long-term phase, seen in the top-right subfigure of Fig. 9) and the maximum pressure generated by combustion.

Fig. 10 illustrates the relationship between the normalized peak combustion pressure, $P_{\max}/P_{\text{initial}}$, and the hydrogen concentration. The peak pressure ratio represents the ratio of the global peak containment pressure after combustion to the initial pressure. The combustion peak pressure ratio can be estimated using a simplified method based on the ideal gas law,

$$\frac{P_{\max}}{P_{initial}} = \frac{n_{\max} T_{\max}}{n_{initial} T_{initial}}, \tag{19}$$

where the subscript max denotes the value at the time of pressure peaking.

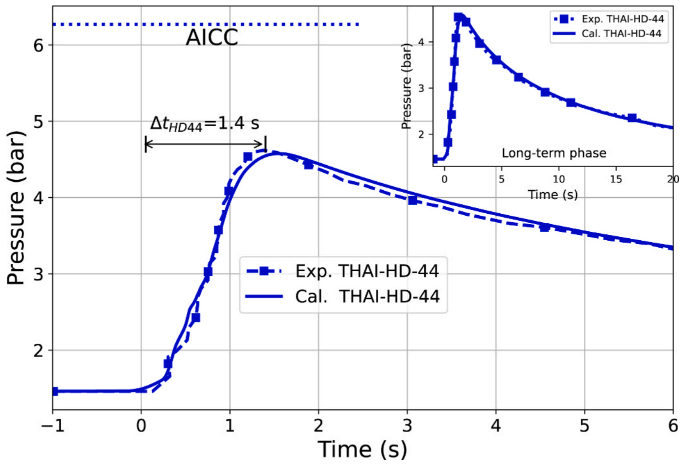

Fig. 9. Pressure transient during the H_2 deflagration and vessel cool-down.

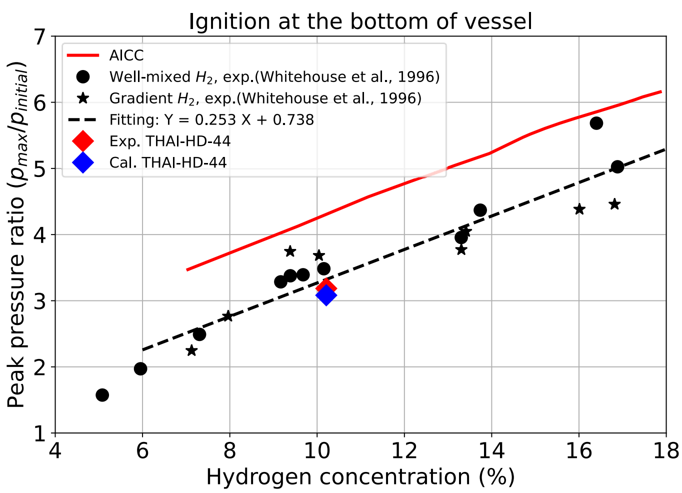

Fig. 10. Peak pressure ratio of lean premixed H_2 combustion.

This simplified method is valid when the mole number and temperature of the burned gas are known. It can be useful for a rough estimation when heat loss is disregarded or when the combustion is adiabatic. However, in real combustion scenarios, the convection and radiation heat transfer to the vessel walls should not be ignored. This is due to the high velocity and temperature of the combustion products. In some cases, steam may also condense on the cold vessel walls.

Based on experimental data on the combustion pressure ratios of well-mixed hydrogen and concentration gradient hydrogen ignited at the bottom of a test vessel (Whitehouse et al., 1996), it has been observed that the peak pressure ratio increases approximately linearly with the hydrogen concentration (Wang et al., 2022b). The experimental data fitting line is,

$$\frac{P_{\max}}{P_{initial}} = 0.253C + 0.738, \tag{20}$$

where C is the hydrogen concentration, vol%.

The combustion pressures are bounded by the AICC (Adiabatic Isochoric Complete Combustion) pressure. This represents the theoretical maximum pressure that can be achieved from the complete burning of a specific amount of hydrogen in a vessel with a constant volume, without any heat loss through the vessel walls. The peak combustion pressure ratios observed in the test and calculation of HD-44, marked as diamonds in Fig. 10, can be approximated by the linear fitting line. However, the fitting line slightly overestimates the peak combustion pressure ratios. In the test, there are two vessels connected by pipes and the heat transfer area per unit volume of the gas mixture is larger compared to the reference one-vessel experiment (Whitehouse et al., 1996). The current estimation method has a significant limitation. It is highly recommended to consider the heat transfer, as well as the turbulence intensity, into the correlation used for predicting the peak combustion pressure, i.e., $\frac{P_{\max}}{P_{initial}} = f\left(C_{H_2}, heat\ transfer, u_t^{'}, \ldots\right)$.

4.3. Temperature transient

The temperature response directly reflects the balance between combustion heat release and heat loss through heat transfer, including convection, radiation, and very little phase change, to the walls of the vessel, as shown in Fig. 12. In test HD-44, two representative temperature distributions in the TTV at elevations of 1.4 m (0.9 m above the igniter) and 7.7 m, as well as two examples in the PAD at elevations of 2.8 m and 7.0 m, are plotted in Fig. 11.

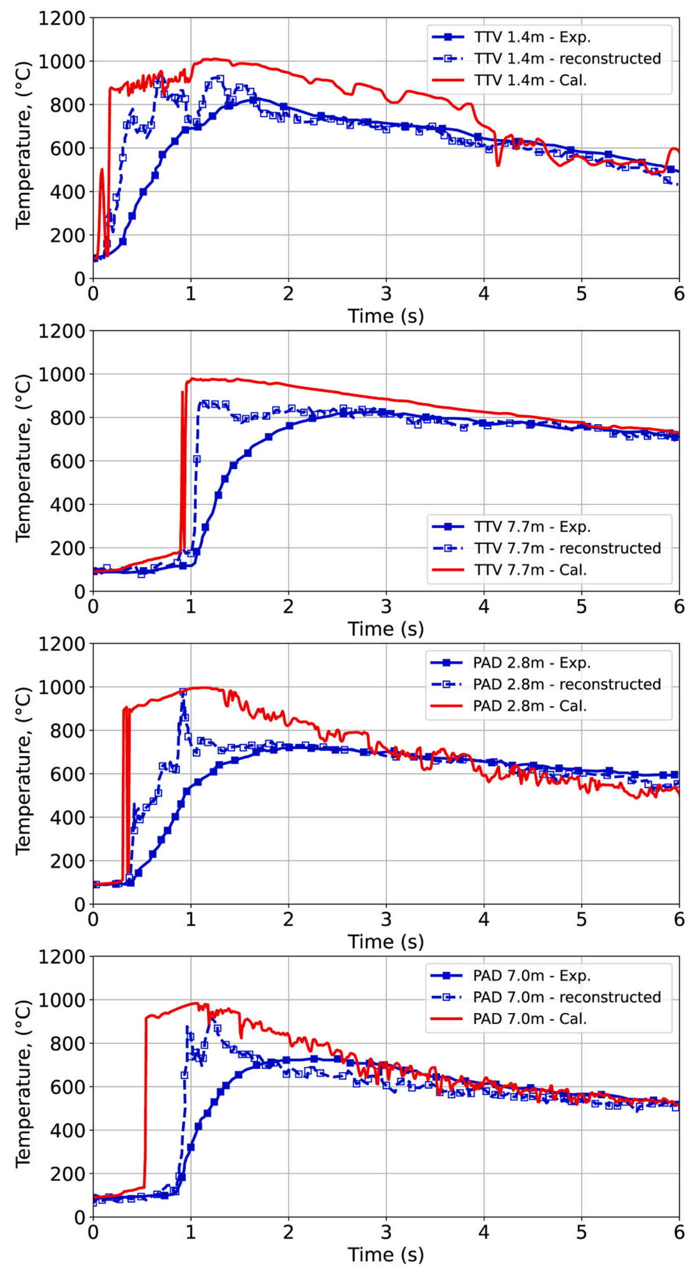

Fig. 11. Temperature evolution in vessels of HD-44 test.

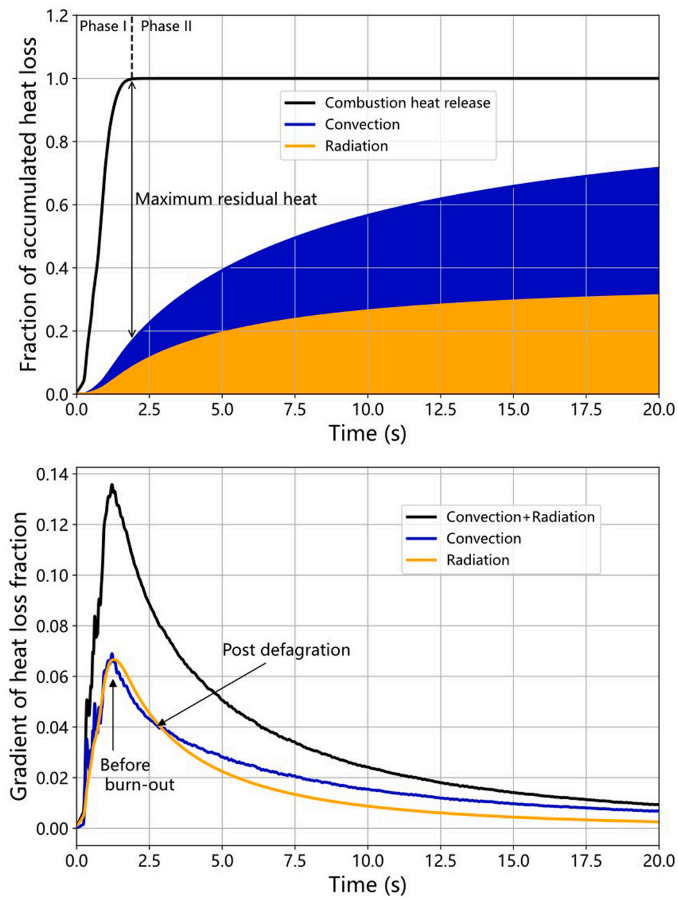

Fig. 12. Fraction and its gradient of the accumulated heat losses in test HD-44.

According to the response time of approximately 210 ms for the thermocouples, the measured temperature profiles generally appear smoother compared to the calculated results. In the calculated results, there is a sharp temperature gradient at the flame front due to the gas heating up rapidly in a short chemical reaction time. Inside the TTV vessel, at the elevation of 1.4 m, the simulated peak temperature is around 1000 °C, while the measured peak temperature is about 830 °C. However, the measured peak temperature could potentially be higher in reality due to the response time of the thermocouples.

To estimate the actual peak temperature, the measured values are reconstructed by assuming that the thermocouple acts as a first-order lag element due to thermal inertia (Freitag and Sonnenkalb, 2019). During the hydrogen combustion phase leading up to the temperature peak, the simulated temperatures along both the TTV and PAD vessel axes, including the steep temperature increase and the peak, closely resemble the reconstructed test results. The simulation results for the maximum gas temperature are approximately 15–25% higher than the measurements, but less than 10% compared to the reconstruction.

During the vessel cool-down phase, the heat transfer (mainly radiation and convection, seen in Fig. 12) from the gas to the vessel walls reduces the temperature. In this phase, all predictions align well with the experimental data. The temperature trend inside the PAD vessel closely resembles that of the TTV vessel. However, the temperature decreases more rapidly in the PAD vessel compared to the TTV vessel. This faster temperature decay is attributed to the smaller diameter of the PAD vessel, which results in a larger heat transfer area per unit volume of the combustible mixture and increased flow velocity. These factors enhance the heat transfer from the gas to the walls through convection and radiation.

4.4. Heat loss

To analyze the balance of heat release and loss during the hydrogen deflagration process in test HD-44, the heat production and dissipation are plotted in Fig. 12. Phase I in Fig. 12 represents the hydrogen deflagration, during which approximately 99% of the hydrogen is burned. The heat release exhibits a sharp increase, reaching its maximum upon the completion of deflagration. However, the total heat loss shows a gradual but slower increase compared to the heat release. In Phase I, the residual heat in the two-vessel system, representing the difference between total heat release and total heat dissipation, increases over time. Consequently, the pressure rises correspondingly, reaching a maximum approximately in 2 s in HD-44 simulation, until the residual heat begins to decrease. At the time corresponding to the largest residual heat, where the peak pressure occurs, the heat dissipation accounts for close to 20% of the total. Subsequently, in phase II (post-deflagration) shown in Fig. 12, the heat loss increases gradually. By 20 s in HD-44, approximately 70% of the total heat generated during the deflagration is lost. The significant temperature difference between the gas and walls underscores the importance of heat loss for predicting pressure response, especially in the post-deflagration phase.

The primary cause of heat loss is convection heat transfer and thermal radiation, with phase change playing a minor role due to the superheated atmosphere. The contributions of these heat transfer mechanisms are illustrated in Fig. 12. Evidently, during Phase I, thermal radiation heat transfer dominates, constituting 60–70% of the overall heat loss. In contrast, in phase II, the contribution from thermal radiation decreases while that from convection increases, as the hydrogen deflagration ceases, leading to a decrease in gas temperature. However, even in phase II, thermal radiation remains comparable to convection. Furthermore, in Phase I, but before burn-out, the gradients of thermal radiation and convection heat transfer exhibit linearly increasing trends, driven by the rising gas temperature and velocity during deflagration. Thermal radiation $\propto T_g^4$ is significantly higher than convective heat transfer $\propto \Delta T \bullet u$, however, both heat losses increase with quite similar linear slopes. On the other hand, in the late phase II, the decreasing gas temperature results in a smaller increase gradient for thermal radiation compared to convection. Consequently, thermal radiation and convective heat transfer emerge as the primary heat-loss mechanisms for predicting pressure response during the experiments, underscoring their importance in numerical simulations. This insight is crucial for setting up accurate heat transfer models in other CFDs and lumped parameter codes (often used in the nuclear safety field) to reproduce test simulations effectively.

5. Conclusions

The theme of this article aims to investigate the concerns of hydrogen deflagration in hydrogen- and nuclear-safety. The THAI-HD-44 hydrogen deflagration experiment in a closed two-compartment system is conducted and simulated by GASFLOW-MPI. Conclusions are drawn from the simulation and experiment as follows,

- Investigations highlight the significance of turbulence in hydrogen deflagration. In cases where there is intense turbulent fluctuation upstream, the hydrogen flame propagates in the opposite direction of the gas flow.
- The pressure rises up to a maximum in less than 2 s, and the temperature exhibits a steep increase and reaches a peak in the reconstructed measurement closely aligning with calculated results.
- A qualitative representation of gas mixture flammability and combustion regime can be achieved in Shapiro and Borghi diagrams using gas concentrations and turbulence intensity, respectively.
- Utilizing the LES turbulence model and the Zimont turbulent flame speed closure to simulate the premixed lean H_2 deflagration test with

a developed initial turbulence, shows good agreement with experimental measurements in terms of flame propagation and deflagration consequences.

- The peak deflagration pressure of premixed lean hydrogen experiences a significant increase with hydrogen concentration. To predict the peak combustion pressure accurately, it is recommended to consider factors such as heat transfer and turbulence intensity, additionally.
- The system heat loss of radiation and convection, leading to vessel cool-down, causes a decrease in system temperature and pressure after deflagration. The long-term phase of hydrogen deflagration pressure load is governed by heat transfer and dissipation in structures. Thermal radiation and convection serve as the main and comparable heat-loss mechanisms for predicting the pressure peak and trend.

Our future efforts will center on experimentally measuring flame of H_2 with high volume fraction, and aim to formulate a turbulent combustion model incorporating the dilute steam effect.

Declaration of Competing Interest

The authors declare that they have no known competing financial interests or personal relationships that could have appeared to influence the work reported in this paper.

Acknowledgements

The HD-44 test was conducted in the frame of OECD/NEA THAI-3 project (2016–2019). The financial support of the participating countries and German Federal Ministry for Economic Affairs and Energy (BMWi) to the OECD/NEA THAI-3 project is gratefully acknowledged.

Appendix A. Supporting information

Supplementary data associated with this article can be found in the online version at doi:10.1016/j.psep.2024.01.101.

References

Berman, M., 1986. A critical review of recent large-scale experiments on hydrogen-air detonations. Nucl. Sci. Eng. 93 (4), 321–347.
Bleyer, A., Taveau, J., Djebaïli-Chaumeix, N., Paillard, C.E., Bentaïb, A., 2012. Comparison between FLACS explosion simulations and experiments conducted in a PWR Steam Generator casemate scale down with hydrogen gradients. Nucl. Eng. Des. 245, 189–196.
Borghi, R., 1990. Turbulent premixed combustion: further discussions on the scales of fluctuations. Combust. Flame 80 (3-4), 304–312.
Boudier, P., Henriot, S., Poinsot, T., Baritaud, T., 1992. A model for turbulent flame ignition and propagation in spark ignition engines (January). In: In Symposium (International) on Combustion, Vol. 24. Elsevier, pp. 503–510 (January).
Chandrasekhar, S., 1960. Radiative Transfer. Dover Publications, New York.
Coward, H.F., Jones, G.W., 1952. Limits of flammability of gases and vapors, Vol. 503. US Government Printing Office.
Crowl, D.A., Jo, Y.D., 2007. The hazards and risks of hydrogen. J. Loss Prev. Process Ind. 20 (2), 158–164.
Damköhler, G., 1940. Z. Elektrochem. Angew. Phys. Chem. 46 (1940), 601–626.
Faix-Gantier, A., 2001. Phénoménologie et calculs numériques de la propagation d'une flamme prémélangée hydrogène-air pauvre dans un milieu turbulent (Doctoral dissertation, Poitiers).
Freitag, M.; Sonnenkalb, M., 2019. Comparison report for blind and open simulation of HD-44, Technical Report 150 1516-CR-HD44, Becker Technologies GmbH, Eschborn, December, 2019.
Freitag, M., Kühnel, A., Langer, G., 2016. Extension of the Thai Test Facility by a Second Vessel: PAD: Technical Report - Reactor Safety Research - Project No. 1501455. 1501455 e FB/TR e THAIPLUS, Becker Technologies GmbH, Eschborn, 2016.
Freitag, M.; Schmidt, E.; Langer, G., 2018. Hydrogen combustion and flame propagation in two-compartment system, Technical Report 150 1516-TR/FB- HD40–45, Becker Technologies GmbH, Eschborn, December, 2018.
Gerke, U., Boulouchos, K., 2012. Three-dimensional computational fluid dynamics simulation of hydrogen engines using a turbulent flame speed closure combustion model. Int. J. Engine Res. 13 (5), 464–481.
Gupta, S., Freitag, M., Poss, G., 2021. THAI experimental research on hydrogen risk and source term related safety systems. Front. Energy 1–29.
Halouane, Y., Dehbi, A., 2017. CFD simulations of premixed hydrogen combustion using the eddy dissipation and the turbulent flame closure models. Int. J. Hydrog. Energy 42 (34), 21990–22004.
Hassan, Y.A., 2008. Large eddy simulation in pebble bed gas cooled core reactors. Nucl. Eng. Des. 238 (3), 530–537.
Kim, S.I. and Kim, Y., 2019. Review: Hydrogen Tank Explosion in Gangneung, South Korea, Proceeding: 2019 Center for Hydrogen Safety Conference.
Langella, I., Doan, N.A.K., Swaminathan, N., Pope, S.B., 2018. Study of subgrid-scale velocity models for reacting and nonreacting flows. Phys. Rev. Fluids 3 (5), 054602.
Launder, B.E., Rodi, W., 1983. The turbulent wall jet measurements and modeling. Annu. Rev. Fluid Mech. 15 (1), 429–459.
Lipatnikov, A.N., Chomiak, J., 2002. Turbulent flame speed and thickness: phenomenology, evaluation, and application in multi-dimensional simulations. Prog. Energy Combust. Sci. 28 (1), 1–74.
Magnussen, B.F., Hjertager, B.H., 1977. On mathematical modeling of turbulent combustion with special emphasis on soot formation and combustion (January). In: In Symposium (international) on Combustion, Vol. 16. Elsevier, pp. 719–729 (January).
Metghalchi, M., Keck, J.C., 1982. Burning velocities of mixtures of air with methanol, isooctane, and indolene at high pressure and temperature. Combust. Flame 48, 191–210.
Nie, Z., Gao, W., Jiang, H., Zhao, F., Zheng, G., Zhang, Z., 2023. Flameless venting characteristics of hydrogen explosion under the coupling of carbon dioxide and metal foam. Process Saf. Environ. Prot. 180, 375–385.
OECD/NEA, 2010. Summary report of the OECD/NEA THAI Project: Hydrogen and Fission Product Issues Relevant for Containment Safety Assessment under Severe Accident Conditions, NEA/CSNI/R(2010)3, June (2010).
Piomelli, U., 1999. Large-eddy simulation: achievements and challenges. Prog. Aerosp. Sci. 35 (4), 335–362.
Povilaitis, M., Jaseliūnaitė, J., 2021. Simulation of hydrogen-air-diluents mixture combustion in an acceleration tube with FlameFoam solver. Energies 14 (17), 5504.
Rose, P., 2020. Modeling a potential hydrogen refueling station network for fuel cell heavy-duty vehicles in Germany in 2050. PhD dissertation. Karlsruhe Institute of Technology (KIT),, Germany.
Salmanzadeh, M., Rahnama, M., Ahmadi, G., 2010. Effect of sub-grid scales on large eddy simulation of particle deposition in a turbulent channel flow. Aerosol Sci. Technol. 44 (9), 796–806.
Sathiah, P., Komen, E., Roekaerts, D., 2012. The role of CFD combustion modeling in hydrogen safety management—Part I: Validation based on small scale experiments. Nucl. Eng. Des. 248, 93–107.
Schmid, H.P., Habisreuther, P., Leuckel, W., 1998. A model for calculating heat release in premixed turbulent flames. Combust. Flame 113 (1-2), 79–91.
Shapiro, Z.M., Moffette, T.R., 1957. Hydrogen flammability data and application to PWR loss-of-coolant accident (No. WAPD-SC-545). Westinghouse Electric Corp., Pittsburgh, PA (United States). Bettis Plant.
Siegel, R., Howell, J.R., 1992. Thermal Radiation Heat Transfer. Hemisphere Publishing, Washington.
Smagorinsky, J., 1963. General circulation experiments with the primitive equations: I. The basic experiment. Mon. Weather Rev. 91 (3), 99–164.
Sparrow, E.M., Cess, R.D., 1978. Radiation Heat Transfer. Hemisphere Publishing, Washington.
Wang, F., Xiao, J., Jordan, T., 2022a. GASFLOW-MPI analysis on deflagration in full-scale hydrogen refuelling station experiments: H2-air premixed cloud and high-pressure H2 jet. Int. J. Hydrog. Energy 47 (32), 14725–14739.
Wang, F., Zou, Z., Deng, J., Qin, H., Zhang, M., 2022b. Investigations of hydrogen hazard mitigation by deliberate ignition in small modular reactor during severe accident using GASFLOW-MPI. Ann. Nucl. Energy 179, 109392.
Wang, F., Xiao, J., Kuznetsov, M., Breitung, W., He, B., Rui, S., Zhou, S., Jordan, T., Song, K., Zhang, L., 2023. Deterministic risk assessment: a showcase of hydrogen leak from a fuel cell truck in a real semi-confined refueling station with a large roof. Int. J. Hydrog. Energy, HE_40865. https://doi.org/10.1016/j.ijhydene.2023.09.114.
Whitehouse, D.R., Greig, D.R., Koroll, G.W., 1996. Combustion of stratified hydrogen-air mixtures in the 10.7 m3 combustion test facility cylinder. Nucl. Eng. Des. 166 (3), 453–462.
Xiao, J., Travis, J.R., Kuznetsov, M., 2015. Numerical investigations of heat losses to confinement structures from hydrogen-air turbulent flames in ENACCEF facility. Int. J. Hydrog. Energy 40 (38), 13106–13120.
Xiao, J., Travis, J.R., Royl, P., Necker, G., Svishchev, A., Jordan, T., 2016. Three-dimensional all-speed CFD code for safety analysis of nuclear reactor containment: Status of GASFLOW parallelization, model development, validation and application. Nucl. Eng. Des. 301, 290–310.
Xiao, J., Breitung, W., Kuznetsov, M., Zhang, H., Travis, J.R., Redlinger, R., Jordan, T., 2017. GASFLOW-MPI: a new 3-D parallel all-speed CFD code for turbulent dispersion and combustion simulations: Part I: Models, verification and validation. Int. J. Hydrog. Energy 42 (12), 8346–8368.
Zhang, H., Li, Y., Xiao, J., Jordan, T., 2017. Large eddy simulation of turbulent flow using the parallel computational fluid dynamics code GASFLOW-MPI. Nucl. Eng. Technol. 49 (6), 1310–1317.
Zimont, V.L., 1979. Theory of turbulent combustion of a homogeneous fuel mixture at high Reynolds numbers. Combust. Explos. Shock Waves 15 (3), 305–311.
Zimont, V.L., 2000. Gas premixed combustion at high turbulence. Turbulent flame closure combustion model. Exp. Therm. Fluid Sci. 21 (1-3), 179–186.